VASCULAR BIOLOGY

Voltage-dependent Ca^{2+} entry into smooth muscle during contraction promotes endothelium-mediated feedback vasodilation in arterioles

Christopher J. Garland,* Pooneh Bagher,*† Chloe Powell, Xi Ye, Hamish A.L. Lemmey, Lyudmyla Borysova, Kim A. Dora‡

Vascular smooth muscle contraction is suppressed by feedback dilation mediated by the endothelium. In skeletal muscle arterioles, this feedback can be activated by Ca^{2+} signals passing from smooth muscle through gap junctions to endothelial cells, which protrude through holes in the internal elastic lamina to make contact with vascular smooth muscle cells. Although hypothetically either Ca^{2+} or inositol trisphosphate (IP_3) may provide the intercellular signal, it is generally thought that IP_3 diffusion is responsible. We provide evidence that Ca^{2+} entry through L-type voltage-dependent Ca^{2+} channels (VDCCs) in vascular smooth muscle can pass to the endothelium through positions aligned with holes in the internal elastic lamina in amounts sufficient to activate endothelial cell Ca^{2+} signaling. In endothelial cells in which IP_3 receptors (IP_3Rs) were blocked, VDCC-driven Ca^{2+} events were transient and localized to the endothelium that protrudes through the internal elastic lamina to contact vascular smooth muscle cells. In endothelial cells in which IP_3Rs were not blocked, VDCC-driven Ca^{2+} events in endothelial cells were amplified to form propagating waves. These waves activated voltage-insensitive, intermediate-conductance, Ca^{2+}-activated K^+ (IK_{Ca}) channels, thereby providing feedback that effectively suppressed vasoconstriction and enabled cycles of constriction and dilation called vasomotion. Thus, agonists that stimulate vascular smooth muscle depolarization provide Ca^{2+} to endothelial cells to activate a feedback circuit that protects tissue blood flow.

INTRODUCTION

Autoregulation of tissue blood flow is crucial for normal physiological function. This fundamental response depends on myogenic tone, an ongoing pressure-induced vascular smooth muscle cell contraction in small arteries that can be rapidly modulated by perivascular nerves, autacoids, the extracellular accumulation of metabolites, and the endothelium (*1*, *2*). Myogenic tone is underpinned by increases in intraluminal pressure depolarizing vascular smooth muscle and increasing the open probability of L-type voltage-dependent Ca^{2+} channels (VDCCs) (*3*, *4*). The L-type VDCC in smooth muscle is the $Ca_V1.2$ isoform, which is activated by Bay K8644 (BayK) and inhibited by nifedipine (*5*, *6*).

In cerebral arteries, myogenic tone is continuously suppressed by an intracellular signaling pathway intrinsic to smooth muscle that helps ensure constant blood flow. Ca^{2+} sparks, generated by Ca^{2+} release through ryanodine receptors (RyRs) adjacent to the plasmalemma, activate large-conductance voltage- and Ca^{2+}-activated K^+ (BK_{Ca}) channels, reducing the open probability of VDCCs, limiting Ca^{2+} influx, and suppressing contraction (*7*, *8*). This negative feedback mechanism reduces excessive cerebral artery constriction, thereby preserving blood flow and protecting against neuronal hypoxia. However, opposing myogenic tone to this extent is not a physiological priority in skeletal muscle, where high resistance to blood flow is necessary at rest yet increased flow must be accommodated during exercise. Consistent with this difference, Ca^{2+} sparks are absent from smooth muscle cells of smaller, second-order pressurized skeletal muscle arterioles although myogenic tone is present. Furthermore, although smooth muscle BK_{Ca} channel activation can suppress contraction, these channels do not seem to be subject to the same tight intracellular regulation as cerebral smooth muscle cells (*9*–*11*).

In addition to intracellular control, negative feedback also operates between vascular cells. Specifically, intercellular Ca^{2+} signaling from activated vascular smooth muscle to endothelial cells (myoendothelial signaling) suppresses vasoconstriction because increases in endothelial cell Ca^{2+} stimulate vasodilation. Thus, α_1-adrenoceptor stimulation or direct depolarization with high extracellular KCl leads to increased endothelial cell $[Ca^{2+}]_i$, causing nitric oxide release to limit vasoconstriction (*12*). Similar myoendothelial signaling and feedback in response to adrenergic agonists operates in other vascular beds and can also involve endothelium-dependent hyperpolarization (EDH) and cycles of contraction and dilation termed vasomotion (*13*–*18*). In both cases, endothelial cells are activated by a signal passing from smooth muscle through myoendothelial gap junctions. Both inositol trisphosphate (IP_3) and Ca^{2+} can, in theory, pass through these gap junctions, and it has been argued that paracrine signaling is due solely to IP_3 movement into the endothelium to activate Ca^{2+} wavelets (*17*, *19*). These Ca^{2+} events are termed pulsars if they align within or near holes in the internal elastic lamina, the only possible sites of myoendothelial gap junctions (*13*, *14*, *16*). However, data supporting this assertion are based on an assumption of IP_3 movement and the use of nonspecific pharmacological tools. The movement of IP_3 may be spatially and temporally far more restricted than previously thought (*20*–*22*), reopening the debate as to whether Ca^{2+} itself might act as an effective signal between cells by passing through gap junctions.

The possibility that Ca^{2+} may pass from smooth muscle in amounts sufficient to activate endothelial cell Ca^{2+} events and initiate feedback has not been explored or seriously considered (*17*). We showed in skeletal muscle arterioles that Ca^{2+} in smooth muscle could pass to the endothelium through positions aligned with holes in the internal elastic lamina in amounts sufficient to activate endothelial cell Ca^{2+} signaling.

Department of Pharmacology, University of Oxford, Mansfield Road, Oxford OX1 3QT, UK.
*Joint first authors.
†Present address: Department of Medical Physiology, College of Medicine, Texas A&M University Health Science Center, 702 Southwest H.K. Dodgen Loop, Temple, TX 76504, USA.
‡Corresponding author. Email: kim.dora@pharm.ox.ac.uk

To demonstrate this phenomenon, we loaded endothelial cells in pressurized arterioles with heparin to antagonize the effect of IP_3 and then opened L-type VDCCs in the smooth muscle with BayK to stimulate Ca^{2+} influx. BayK evoked a new, elementary Ca^{2+} event, VDCC-dependent Endothelial cell Ca^{2+} Transients (we term VECTors), which could evolve into endothelial cell Ca^{2+} pulsars and "waves" through IP_3 receptor (IP_3R)–dependent Ca^{2+}-induced Ca^{2+} release. These directional Ca^{2+} signals from smooth muscle then stimulated voltage-insensitive, intermediate-conductance, Ca^{2+}-activated K^+ (IK_{Ca}) channels localized within the endothelial cell membrane projections to the smooth muscle, leading to suppression of agonist-induced vasoconstriction and initiating the dilation phase of vasomotion.

RESULTS

Direct activation of arteriole L-type VDCCs with BayK triggers myoendothelial Ca^{2+} signaling

Arterioles from rat cremaster had a maximum diameter of 163 ± 1 μm and developed ~50% pressure-induced myogenic tone, which was abolished by blocking L-type VDCCs with nifedipine (fig. S1). Endothelial cells loaded with a Ca^{2+} indicator (OGB-1) were visible at the bottom plane of pressurized arterioles with myogenic tone (Fig. 1A and fig. S2A). Ca^{2+} events were analyzed manually (*1*), because automated analysis did not provide complete or reliable data (fig. S2, B to D). To assess whether directly opening L-type VDCCs influenced endothelial cell [Ca^{2+}], we used two concentrations of BayK in the absence and presence of nifedipine (Fig. 1, A and B). At 3 nM, BayK increased the frequency of endothelial cell Ca^{2+} events fourfold without affecting arteriolar diameter (Fig. 1, A and C, fig. S3A, and movie S1), and recruited new active sites, doubling the percentage of active cells (Fig. 1D). Cumulative addition of BayK to a final concentration 30 nM stimulated robust vasoconstriction and vasomotion (movie S1), and further increased Ca^{2+} event frequency to 10-fold above baseline (Fig. 1, A and C). Nearly all cells were now active, threefold more than at baseline (Fig. 1D and movie S1). As expected, blocking L-type VDCCs with nifedipine prevented vasoconstriction and the activation of endothelial cell Ca^{2+} events in response to either concentration of BayK (Fig. 1, B to D). Inhibition of contraction with blebbistatin prevented the development of myogenic tone (contraction) without affecting the ability of BayK to activate endothelial cell [Ca^{2+}] (fig. S3, A to C), suggesting that the diameter of arterioles per se did not influence endothelial cell [Ca^{2+}].

As we have previously shown (*1*), spontaneous (in the absence of BayK) endothelial cell Ca^{2+} events occurred mainly as localized Ca^{2+} increases, radiating less than ~10 μm from the center of an event, and were insensitive to nifedipine (Fig. 1, C and D, and fig. S4, A and B).

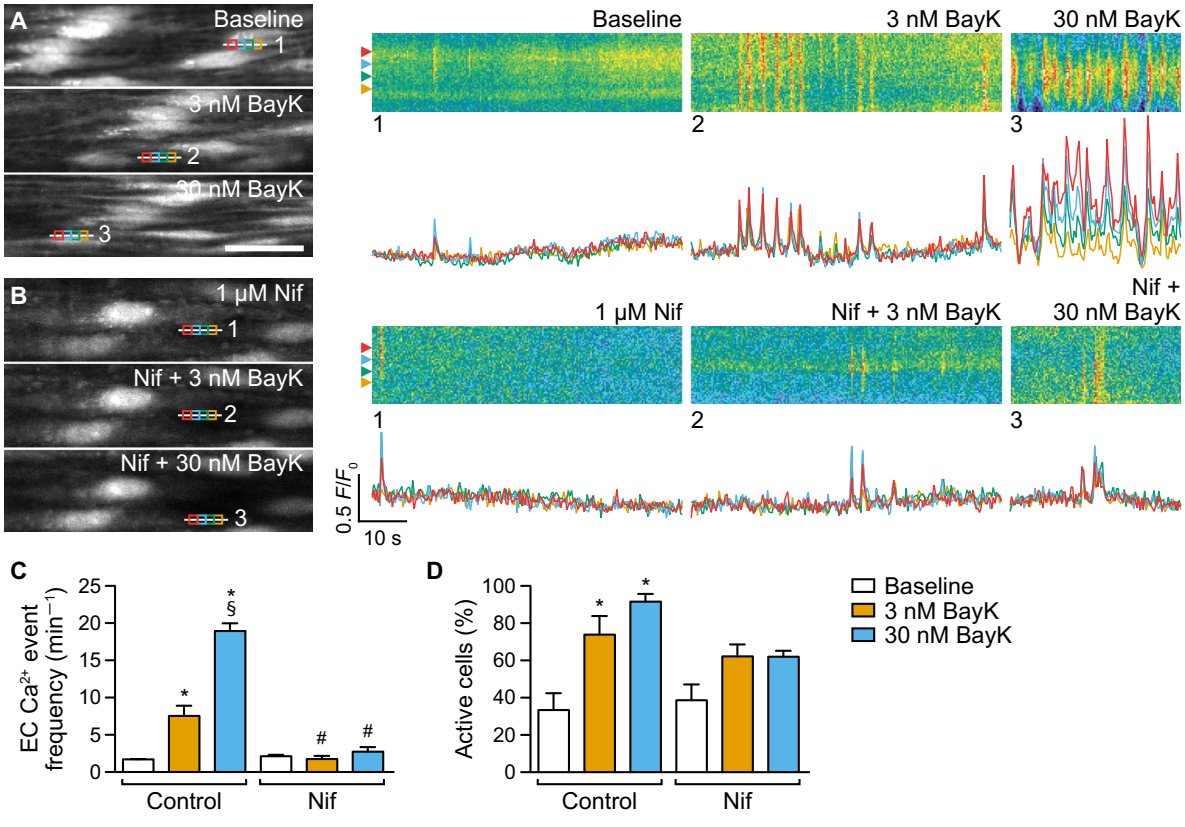

Fig. 1. Direct activation of L-type VDCCs in arterioles with BayK increases Ca^{2+} events in endothelial cells. (**A** and **B**) Confocal fluorescence images of endothelial cells (ECs) loaded with the Ca^{2+} indicator OGB-1 viewed at the bottom plane in pressurized arterioles with myogenic tone in the absence (A) and presence (B) of nifedipine (Nif), at baseline and with the indicated concentrations of the L-type VDCC agonist BayK (movie S1); scale bar, 30 μm. Representative fluorescence intensity data shown as line scans [corresponding to white lines 1 to 3 in (A) or (B)] and fluorescence traces [F/F_0; corresponding to colored subcellular regions of interest (ROIs) in the images]. (**C** and **D**) Bar graphs summarize the effect of BayK on the frequency of EC Ca^{2+} events in active cells (C) and the overall percentage of active cells (D) in the absence and presence of Nif. Data are means ± SEM (≥10 ECs in each field of view from n = 3 to 6 arterioles from different animals); *P < 0.05 compared with baseline; $^{\#}P$ < 0.05 compared to control; $^{\S}P$ < 0.05 compared to 3 nM BayK.

About a quarter of spontaneous Ca^{2+} events were propagating waves, often covering over half a cell length. Endothelial cell Ca^{2+} events stimulated by 3 nM BayK remained localized, whereas those stimulated by 30 nM BayK were sufficient to form propagating waves (fig. S4, A and B).

Elementary Ca^{2+} events occur in the myoendothelial signaling domain

Rat cremaster arteriolar endothelial cells expressed the genes encoding all three isoforms of IP_3R (*Itpr1* to *Itpr3*), but not those encoding RyRs (*Ryr1* to *Ryr3*) (fig. S5, A and B). We used the pan IP_3R antagonist heparin to assess the role of these IP_3Rs in myoendothelial Ca^{2+} signaling in arterioles (fig. S6, A to D). In endothelial cells, heparin-Cy5 closely aligned with IP_3R1 (Fig. 2A). By simultaneously imaging endothelial cell Ca^{2+} and elastin (Fig. 2B), we found that discrete heparin-insensitive endothelial cell Ca^{2+} events rapidly terminated both temporally (duration, ~1 to 2 s) and radially (total width, <15 μm, often 5 to 10 μm) (Fig. 2C) and were localized to the myoendothelial microdomain found within holes in the internal elastic lamina (Fig. 2D). We defined these localized events as VECTors. Compared to untreated cells, heparin halved the frequency of endothelial cell Ca^{2+} events to 30 nM BayK (Fig. 2E), did not affect the percentage of active cells (Fig. 2F), and halved the incidence of Ca^{2+} waves (Fig. 2G and fig. S4A). In the same cells, the TRPV4 channel agonist GSK1016790A increased endothelial cell Ca^{2+}

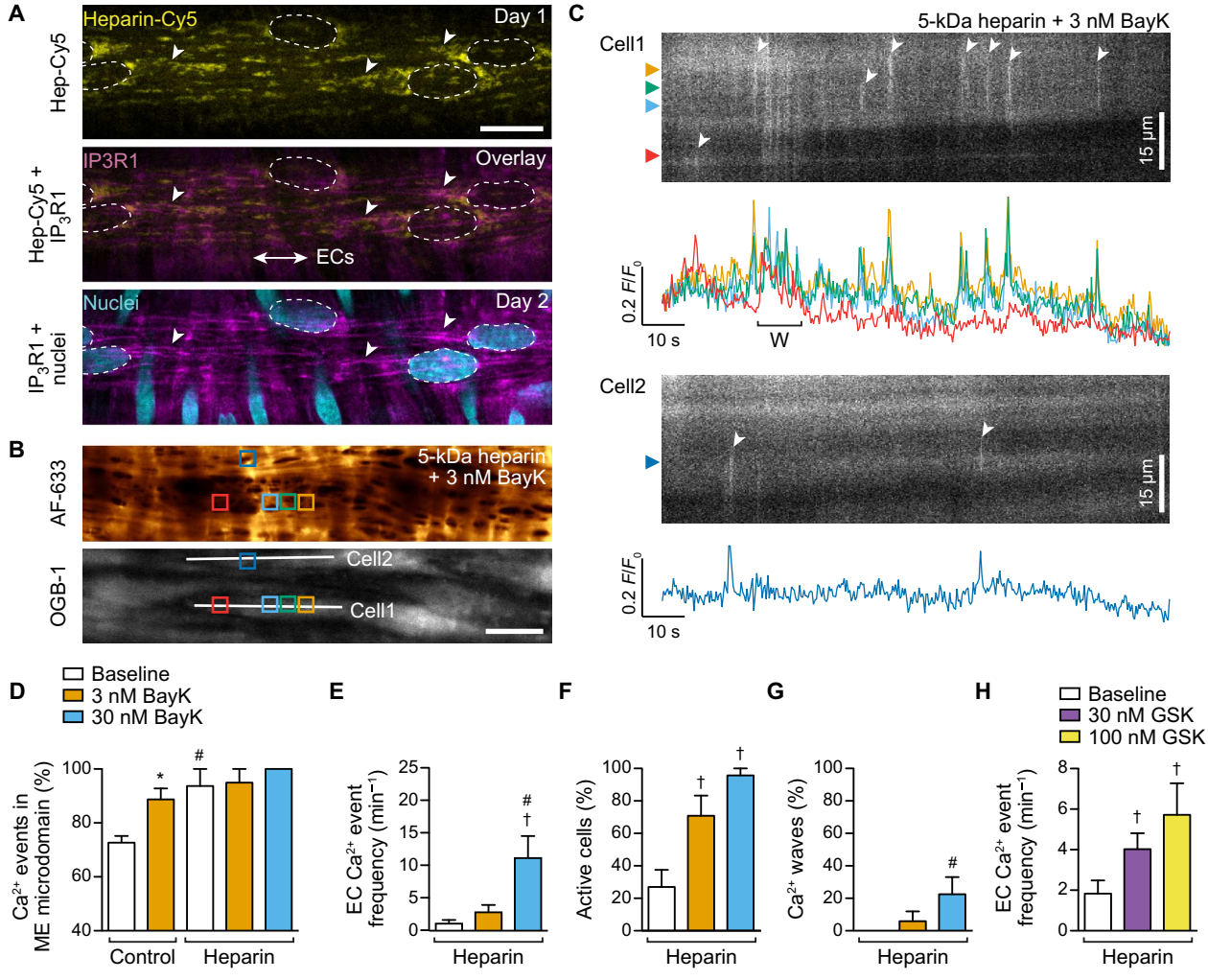

Fig. 2. VECTors occur in myoendothelial microdomains and are amplified by IP_3Rs in endothelial cells. (**A**) Confocal fluorescence images of endothelial cells (ECs) loaded with heparin-Cy5 (yellow) and the corresponding IP_3R1 fluorescence in the same arteriole (magenta). Nuclear staining (cyan) is indicated by dashed lines. Representative of three experiments; scale bar, 15 μm. (**B**) Simultaneous confocal fluorescence images of the internal elastic lamina labeled with AF-633 and ECs loaded with the Ca^{2+} indicator OGB-1 in a pressurized arteriole with myogenic tone during treatment with heparin and BayK; scale bar, 15 μm. (**C**) Representative fluorescence intensity data shown as line scans [corresponding to white lines Cell1 and Cell2 in (B)] and fluorescence traces [F/F_0; corresponding to colored subcellular ROIs in (B)]. Examples of VECTors are indicated by arrowheads. W, wave. (**D**) Bar graph summarizes the effects of BayK on the percentage of EC Ca^{2+} events in the myoendothelial (ME) microdomain visible as holes through the internal elastic lamina. (**E** to **H**) Bar graphs summarize the effect of heparin on the frequency of EC Ca^{2+} events in active cells during BayK (E), the overall percentage of active cells (F), the percentage of these events that propagated along cells and were considered to be waves (G), and subsequent responses to the endothelium-dependent TRPV4 agonist GSK1016790A (GSK) (H). Data are means ± SEM (n = 4 arterioles from different animals); $^*P < 0.05$ compared with baseline; $^{\dagger}P < 0.05$ compared to baseline in the presence of heparin; $^{\#}P < 0.05$ compared to control. (E to G) Control data used for statistical comparisons for BayK are shown in Fig. 1; see (*1*) for control GSK data. Experiments using 5-kDa heparin were only included if the EC Ca^{2+} response to acetylcholine was markedly reduced (fig. S6D).

(Fig. 2H) in a manner similar to control conditions (*1*). Therefore, BayK-induced VECTors are normally amplified by endothelial cell IP_3Rs, first to form puffs and then to propagating cell-wide Ca^{2+} waves.

Attempts to block IP_3Rs with 2-aminoethoxydiphenylborate (2-APB) was complicated by actions at gap junctions, a previously reported effect of this inhibitor (*23*). 2-APB caused arterioles to dilate and contract in an asynchronous manner, supporting an effect on gap junctions (fig. S7A). Furthermore, 2-APB inhibited acetylcholine-mediated dilation (fig. S7B) and feedback dilation induced by BayK application (fig. S7, C and D). In addition, 2-APB blocked dilation mediated by NS309, an allosteric modulator of both isoforms of K_{Ca} channels in endothelial cells, SK_{Ca} (small-conductance, Ca^{2+}-activated K^+) and IK_{Ca} channels, further supporting an effect of 2-APB on myoendothelial gap junctions (fig. S7B). Despite this action at gap junctions, 2-APB blocked the increase in endothelial cell Ca^{2+} normally stimulated by acetylcholine (fig. S7E), supporting an effect on IP_3Rs. Therefore, the ability to block the endothelial cell response to BayK could not reliably be assigned to a single action of 2-APB, yet the block was more complete than with heparin (fig. S7F and Fig. 2E). Overall, the profile of 2-APB block resembled that of heparin, including the ability to confine Ca^{2+} events to the myoendothelial microdomain (fig. S7, G and H). We were unable to use the phospholipase C inhibitor U-73122 against BayK, because it not only blocked dilation to acetylcholine but also prevented contraction to KCl and damaged arterioles (fig. S8A). Similarly, we did not consider the IP_3R1 antagonist xestospongin C (*24*) effective enough to use against BayK (fig. S8B).

BayK does not trigger direct entry of Ca^{2+} into endothelial cells

Freshly isolated endothelial cell tubes were pinned (Fig. 3A) and loaded with Ca^{2+} indicator dye (Fig. 3, B and C). Spontaneous Ca^{2+} events were rare (Fig. 3, D and E) and not altered by either BayK, increased KCl concentration, or the selective α_1-adrenoceptor agonist phenylephrine (Fig. 3, B to E, and movies S2 and S3). However, the muscarinic receptor agonist acetylcholine evoked an increase in Ca^{2+} activity in the same tubes (Fig. 3, B to E). Reverse transcription quantitative polymerase chain reaction (RT-qPCR) analysis showed that the endothelial cell tube mRNA samples were not contaminated with smooth muscle cell mRNA (Fig. 3F) and that mRNAs encoding the $Ca_V1.2$, $Ca_V3.1$, and $Ca_V3.2$ isoforms of L- and T-type VDCCs were detected in whole arterioles, but not endothelial cell tubes (Fig. 3, F and G). Immunolabeling for the smooth muscle isoform of L-type VDCCs, $Ca_V1.2$, revealed punctate labeling in smooth muscle cells but not the endothelium (Fig. 3, H and I), consistent with the mRNA results.

Depolarization stimulates endothelial cell Ca^{2+} events

Other approaches were used to open L-type VDCCs and assess endothelial cell Ca^{2+} activity. Endothelial cell Ca^{2+} activity was increased by depolarization with KCl at a concentration predicted to clamp the membrane potential at −40 mV or the application of the voltage-dependent K^+ (K_v) channel blocker 4-aminopyridine. A clear threshold for the initiation of increased endothelial cell Ca^{2+} activity (Ca^{2+} trigger point) was evident during the time course of vasoconstriction to KCl (movie S4). The frequency of Ca^{2+} events increased 11-fold, and Ca^{2+} events were observed in twice as many endothelial cells, and as predicted, nifedipine blocked the increase in Ca^{2+} events to KCl (Fig. 4, A to D). 4-Aminopyridine also increased the frequency of endothelial cell Ca^{2+} events (a greater than threefold increase), which remained localized and relied on VDCCs (Fig. 4, C and D, and movie S5). In smooth

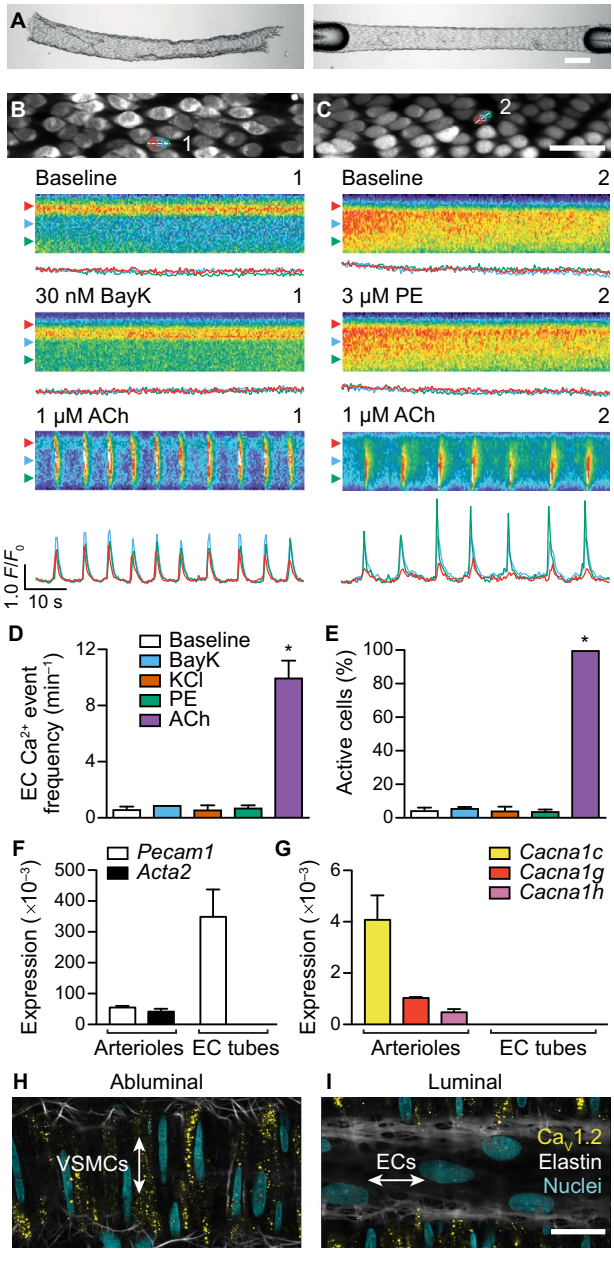

Fig. 3. Lack of L-type VDCCs in arteriolar endothelium. (**A**) Bright-field images of a freshly isolated (left) and pinned (right) endothelial cell (EC) tube isolated from a skeletal muscle arteriole; scale bar, 100 μm. (**B** and **C**) Confocal fluorescence images of two tubes loaded with Fluo-4 to detect Ca^{2+}; scale bar, 30 μm. Representative fluorescence intensity data showing both line scans [corresponding to white lines 1 and 2 in (B) and (C)] and fluorescence traces [F/F_0; corresponding to subcellular ROIs on 1 and 2 (colored squares)] in response to either BayK (B; movie S2) or phenylephrine (PE) (C, movie S3) and the muscarinic agonist acetylcholine (ACh). (**D** and **E**) Bar graphs summarize the effects of BayK, KCl, phenylephrine, and ACh on the frequency of EC Ca^{2+} events (D) and the percentage of active cells (E). Data are means ± SEM (n = 3 to 9 EC tubes from different animals); *P < 0.05 compared with baseline. (**F** and **G**) Bar graphs summarize the gene expression for (F) EC (PECAM-1, *Pecam1*) and smooth muscle cell (α–smooth muscle actin, *Acta2*) markers; and (G) L- and T-type Ca_V channel isoforms ($Ca_V1.2$, *Cacna1c*; $Ca_V3.1$, *Cacna1g*; and $Ca_V3.2$, *Cacna1h*) in arterioles and EC tubes. Data are means ± SEM; n = 4 sets of pooled mRNA samples from four animals. (**H** and **I**) Immunofluorescence for $Ca_V1.2$ (yellow) in a pressurized arteriole; scale bar, 20 μm. Vascular smooth muscle cells (VSMCs) have vertically aligned nuclei (blue), and ECs have horizontally aligned nuclei (blue). Representative of three arterioles from different animals.

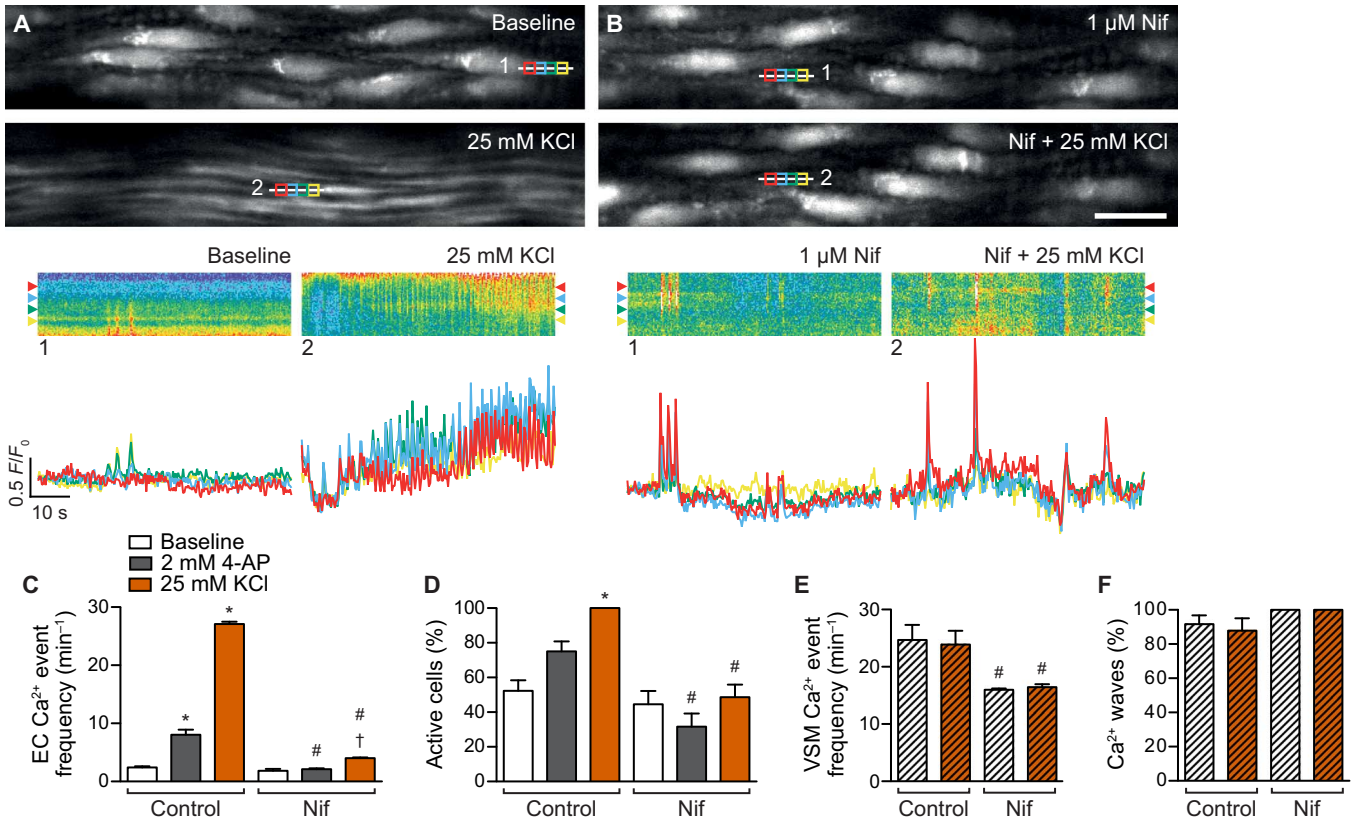

Fig. 4. Depolarization opens VDCCs in smooth muscle and increases Ca^{2+} activity in endothelial cells. (**A** and **B**) Confocal fluorescence images of endothelial cells (ECs) loaded with the Ca^{2+} indicator OGB-1 in pressurized skeletal muscle arterioles with myogenic tone in the absence (A) and presence (B) of nifedipine (Nif), at baseline and with KCl (see also movie S4); scale bar, 30 μm. Representative fluorescence intensity data shown as line scans [corresponding to white lines 1 and 2 in (A) or (B)] and fluorescence traces (F/F_0; corresponding to colored subcellular ROIs in the images). (**C** to **F**) Bar graphs summarize the effect of the K_V channel blocker 4-aminopyridine (4-AP; movie S5) and KCl on the frequency of EC Ca^{2+} events in active cells (C) and the overall percentage of active cells (D), as well as the effects of KCl on the frequency of vascular smooth muscle (VSM) Ca^{2+} events (E) and the percentage of these events that propagated along cells and were considered to be waves (F) in the absence and presence of Nif. Data are means ± SEM (≥10 ECs or VSMCs in each field of view from $n = 3$ to 6 arterioles from different animals); $^{*}P < 0.05$ compared with control baseline; $^{\dagger}P < 0.05$ compared to baseline in the presence of 1 μM Nif; $^{\#}P < 0.05$ compared to control.

muscle, nifedipine prevented localized Ca^{2+} events, preserving pressure-evoked oscillating Ca^{2+} waves, and during contraction, KCl did not alter this profile (Fig. 4, E and F). These smooth muscle Ca^{2+} events, but not endothelial cell Ca^{2+} events, were blocked by ryanodine, which inhibits RyRs (fig. S9, A and B). Therefore, endothelial cell IP_3Rs are responsible for the Ca^{2+}-induced Ca^{2+} release required to transform VECTors into Ca^{2+} puffs and waves.

Smooth muscle α_1-adrenoceptor stimulation evokes endothelial cell Ca^{2+} events

To place these observations in a physiological context, the α_1-adrenoceptor agonist phenylephrine, which depolarizes smooth muscle during contraction, was used to assess endothelial cell Ca^{2+} responses. Two concentrations were used; the contraction to the higher concentration relied less on VDCCs (Fig. 5, A and B, fig. S10, A and B, and movie S6). Either concentration of phenylephrine increased the frequency of endothelial cell Ca^{2+} events 10-fold (Fig. 5C). However, nifedipine did not fully block the Ca^{2+} response to the higher concentration of phenylephrine (Fig. 5C), thus supporting a role for smooth muscle IP_3 in influencing endothelial cell Ca^{2+} and the formation of pulsars (*13*, *14*). The higher concentration of phenylephrine recruited new cells during the response (Fig. 5D). In response to arteriole stimulation with phenylephrine, endothelial cell Ca^{2+} events were more likely to occur as waves (fig. S4, A and B), more so in the presence of nifedipine, which caused a deviation from the normally strong positive correlation ($R^2 = 0.96$) between the frequency of endothelial cell Ca^{2+} events and the percentage of waves (fig. S4B). By simultaneously imaging both endothelial and smooth muscle cells at the arteriolar midplane, we demonstrated differential activation of Ca^{2+} events in each cell type (fig. S11, A to E). Midplane data from endothelial cells (fig. S11, A to C) and smooth muscle cells (fig. S11, A, B, D, and E) were consistent with those measured in cells in focus at the bottom surface of arterioles.

Endothelial cell Ca^{2+} events activate IK_{Ca} channels to suppress vasoconstriction

The impact of Ca^{2+} influx through smooth muscle L-type VDCCs on arteriolar function was probed in arterioles with myogenic tone in the absence and presence of inhibitors (fig. S12A). BayK, KCl, and phenylephrine (Fig. 6, A to C) each stimulated vasoconstriction. The small constriction in response to 3 nM BayK was followed by vasodilation toward and beyond baseline (vasomotion was only observed in two of nine arterioles) (Fig. 6A), and after 5 min, there was minimal effect on diameter. BayK (30 nM) evoked rapid vasoconstriction, which developed into vasomotion as part of the feedback vasodilation in all arterioles

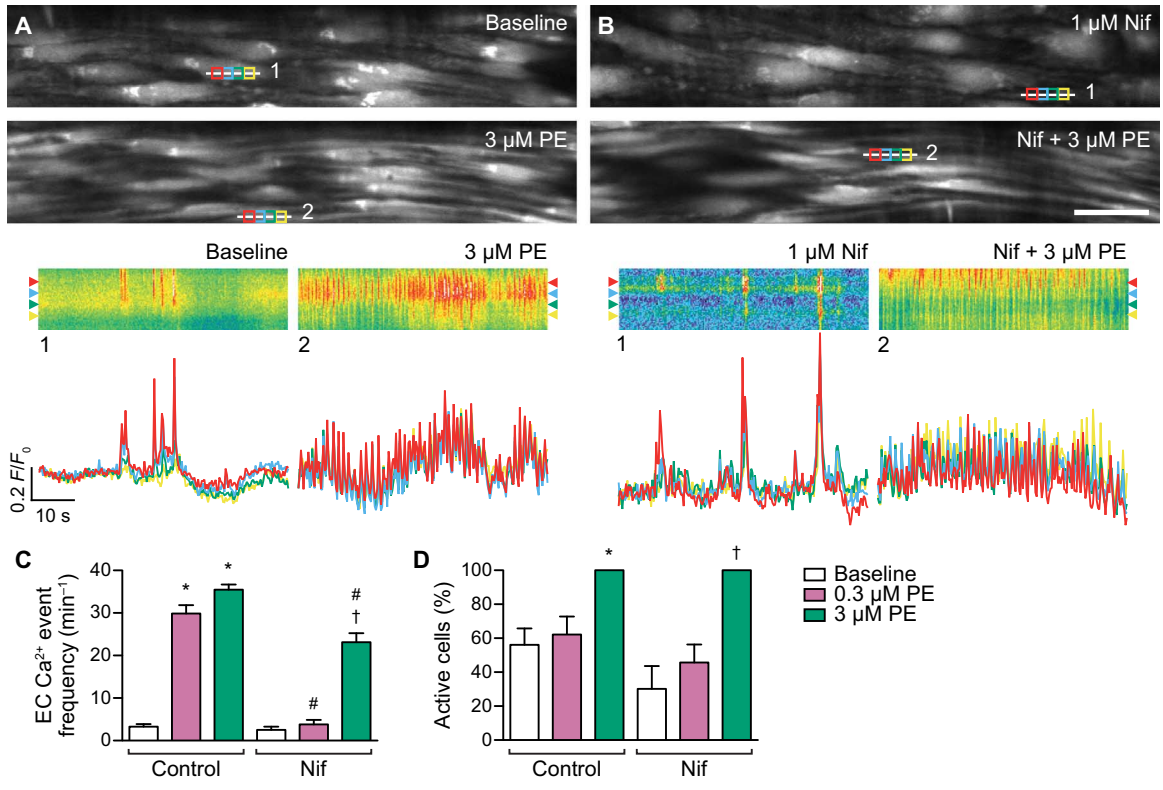

Fig. 5. Activation of α_1-adrenoceptors in smooth muscle increases Ca^{2+} activity in endothelial cells. (**A** and **B**) Confocal fluorescence images of endothelial cells (ECs) loaded with the Ca^{2+} indicator OGB-1 from pressurized arterioles with myogenic tone in the absence (A) and presence (B) of nifedipine (Nif) at baseline and with the α_1-adrenoceptor agonist phenylephrine (PE) (movie S6); scale bar, 30 μm. (**C** and **D**) Representative fluorescence intensity data shown as line scans [corresponding to white lines 1 and 2 in (A) or (B)] and fluorescence traces (F/F_0; corresponding to colored subcellular ROIs in the images). (C and D) Bar graphs summarize the effects of PE on the frequency of EC Ca^{2+} events in active cells (C) and the overall percentage active cells (D) in the absence and presence of Nif. Data are means ± SEM (≥10 ECs in each field of view from $n = 3$ to 4 arterioles from different animals); $^*P < 0.05$ compared with control baseline; $^{\dagger}P < 0.05$ compared to baseline in the presence of 1 μM Nif; $^{\#}P < 0.05$ compared to control.

(Fig. 6A). Blocking nitric oxide synthase with L-NAME did not affect feedback dilation (Fig. 6D) and increased the incidence of vasomotion in response to 3 nM BayK (6 of 11 arterioles, no effect against 30 nM BayK). Despite the apparent lack of involvement of nitric oxide in feedback dilation, the vasodilation phase did reflect endothelium-dependent feedback, because TRAM-34 (which blocks IK_{Ca} channels responsible for EDH) increased the magnitude of vasoconstriction and abolished feedback to both concentrations of BayK (Fig. 6, A and D). Vasomotion was abolished by TRAM-34, and the arterioles remained at the more constricted diameters and did not dilate. In contrast to the vasoconstriction to BayK (and phenylephrine), and to other vascular beds (*12*), contraction to KCl remained stable for over 5 min (Fig. 6, B and D), supporting the crucial importance of operational K^+ channels during feedback and vasomotion in these arterioles. Nifedipine fully blocked vasoconstriction to BayK and KCl (Fig. 6B and table S1).

Vasoconstriction to phenylephrine rapidly peaked and had returned ~35% toward the baseline myogenic tone 5 min after application (Fig. 6C and fig. S12, B to D). This return was also due to endothelium-dependent feedback and was abolished by TRAM-34 or damage to the endothelium, but not by iberiotoxin, a selective blocker of BK_{Ca} channels present in smooth muscle (Fig. 6, C and D, and fig. S12, C, D, and G). These inhibitors did not affect contraction in response to phenylephrine (fig. S12E). As with BayK (Fig. 6A), endothelial IK_{Ca} channels were responsible for the dilation phase of vasomotion to phenylephrine (Fig. 6C and fig. S12F). The endothelium-dependent feedback was not altered by blocking either SK_{Ca} channels (the other K_{Ca} channel in the endothelium) with apamin or nitric oxide synthase with L-NAME (Fig. 6D). However, apamin and L-NAME each increased the incidence of vasomotion during 3 μM phenylephrine (fig. S12F). No feedback occurred during constriction in response to 3 μM phenylephrine in the presence of nifedipine (fig. S10, A and C), further supporting a link between IK_{Ca} channels and L-type VDCCs in suppressing vasoconstriction. Similarly, constriction in response to 0.3 μM phenylephrine was unaffected by L-NAME (although L-NAME increased the incidence of vasomotion from control: 3 of 14 arterioles; L-NAME: 4 of 4 arterioles), and both the feedback dilation and vasomotion were abolished by TRAM-34 alone (Fig. 6, C and D).

The trigger point for activation of endothelial cell Ca^{2+} events by vasoconstrictors can be defined

Arteriolar diameter and specifically inner diameter could be tracked by fluorescently labeling the internal elastic lamina separating the endothelium and smooth muscle with Alexa Fluor 633 hydrazide (AF-633) (Fig. 7, A and B) while simultaneously imaging endothelial cell Ca^{2+} events at the arteriolar midplane (Fig. 7C). During vasoconstriction in response to KCl and phenylephrine, endothelial cell Ca^{2+} events were limited until one or two cells became activated, which was followed shortly by Ca^{2+} oscillations in all endothelial cells, the trigger point for activation of endothelial cell Ca^{2+}. The movement of the arteriolar wall to the point where endothelial cells were triggered into activity was recorded

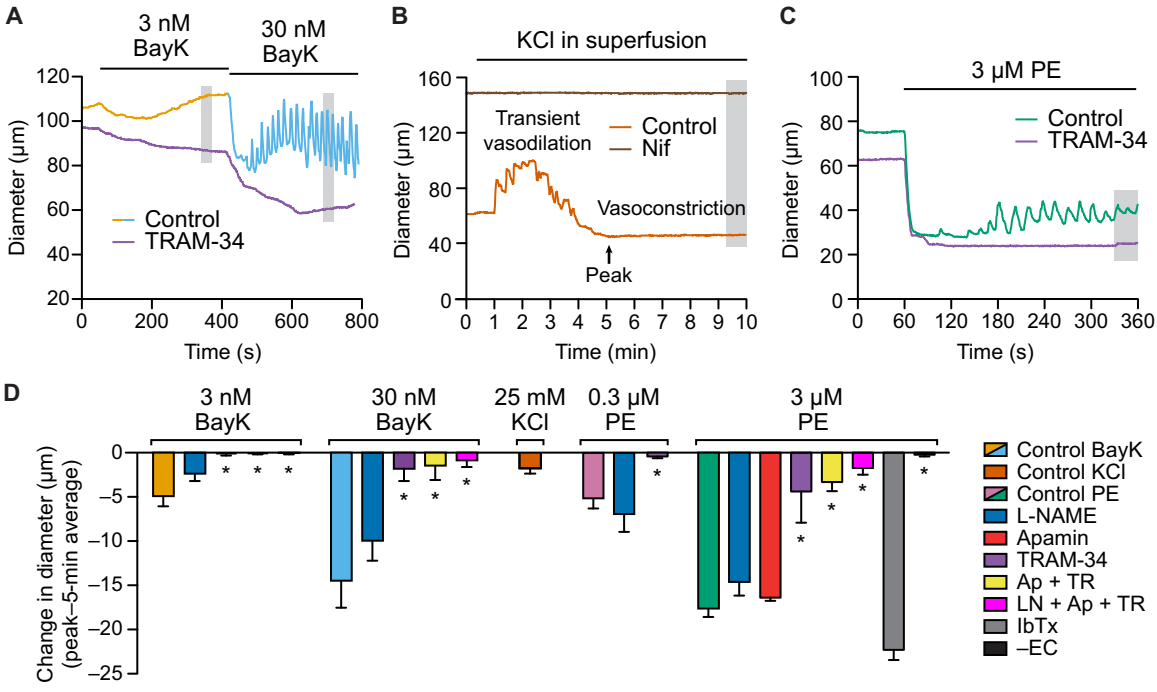

Fig. 6. IK_{Ca} channels in endothelial cells suppress vasoconstriction and initiate vasomotion. (**A** to **C**) Representative diameter traces in pressurized arterioles for (A) single, cumulative exposures to the L-type VDCC agonist BayK before and after incubation (in a separate arteriole) with 1 μM TRAM-34 to block IK_{Ca} channels, as well as consecutive additions of (B) 25 mM isotonic KCl to the superfusion solution in the absence (orange) and presence (brown) of nifedipine (Nif) (1 μM); and (C) the α_1-adrenoceptor agonist phenylephrine in the absence (green) and presence of 1 μM TRAM-34 (purple). (**D**) Bar graphs summarize the effect of the three vasoconstrictors under control conditions; and with 100 μM L-NAME (to block nitric oxide synthase); 100 nM apamin (to block SK_{Ca} channels); 1 μM TRAM-34; apamin and TRAM-34 (Ap + TR); apamin, TRAM-34, and L-NAME (LN + Ap + TR); 100 nM iberiotoxin (IbTx, an inhibitor of BK_{Ca} channels); or in endothelium-denuded arterioles (–EC). Data are means ± SEM (n = 3 to 28 arterioles from different animals); *P < 0.05 compared to the corresponding control response for each vasoconstrictor; 5-min average is indicated by gray bars in (A) to (C). Figure S12 provides more details regarding these experiments.

as distance and extrapolated to an approximate change in diameter (Fig. 7, C and D). At this point, endothelial cell Ca^{2+} events were activated sufficiently to initiate feedback and prevent arterioles from clamping shut. This feedback did not influence myogenic tone per se and could be evoked during minimal further constriction using BayK (Fig. 7D).

DISCUSSION

We showed that in rat cremaster arterioles, an increase in Ca^{2+} could be evoked in the endothelium by activating L-type VDCCs in the adjacent smooth muscle, even by blocking IP_3-mediated endothelial cell Ca^{2+} release with heparin. Overall, our data are consistent with a myoendothelial feedback mechanism activated by Ca^{2+} passing to the endothelium, where IP_3Rs amplify this signal, triggering activation of endothelial cell IK_{Ca} channels and hyperpolarization. Hyperpolarization then feeds back to the smooth muscle, reducing L-type VDCC open probability and relaxing these cells (fig. S13). By driving the dilation phase of vasomotion, the mechanism will prevent a complete loss of blood supply to skeletal muscle, such as during increased sympathetic nerve activity.

Furthermore, the arterioles studied were myogenically active, with myoendothelial feedback only activated when additional L-type VDCCs were recruited, suggesting that Ca^{2+} influx sustaining myogenic tone may be compartmentalized from the Ca^{2+} entry driving endothelium-dependent feedback. Within the microcirculation of skeletal muscle, myogenic tone and responsiveness to sympathetic vasoconstriction combine to create a high vascular resistance, enabling vasodilation to increase blood flow by as much as 100-fold when required (*25*). This range of myogenic tone control is partly explained by decoupled Ca^{2+} sparks and BK_{Ca} channels in smooth muscle cells of skeletal muscle arterioles (*10*, *26*, *27*). Furthermore, in smaller-diameter skeletal muscle arterioles, Ca^{2+} sparks are absent, so although BK_{Ca} channels are present and can suppress contraction, they do not mediate an intracellular negative feedback mechanism (*9*–*11*).

Although either Ca^{2+} or IP_3 has been proposed to diffuse from smooth muscle to stimulate endothelium-dependent feedback dilation (*12*), direct evidence ruling out one or the other was not provided in that original observation. To investigate intercellular signaling further, a vascular coculture of smooth muscle and endothelial cell monolayers linked by myoendothelial projections has been used, allowing independent manipulation of the respective cell types. This approach supports the movement of both Ca^{2+} and IP_3 through myoendothelial gap junctions and in either direction (*28*). Although IP_3 and Ca^{2+} each seem to contribute in the transfer of Ca^{2+} signal from activated smooth muscle to endothelial cells, Ca^{2+} itself transfers in the reverse direction (*28*). This disparity reflects the clustering of IP_3Rs within endothelial cell projections and the generation of Ca^{2+} pulsars, whereas any IP_3 entering the smooth muscle from the endothelium is instead rapidly metabolized (*14*, *29*). Although effective intracellular binding and metabolism limit the ability of Ca^{2+} and IP_3, respectively, to act across multiple cells, their diffusion coefficients, ~13 to 65 and ~10 to 290 $\mu m^2/s$ (*20*, *21*), and the small size of smooth muscle and endothelial cells suggest that both might provide an effective signal. This may particularly be the case for movement from smooth muscle into the very restricted volume presented by the endothelial projections containing IP_3Rs (*14*, *17*) to

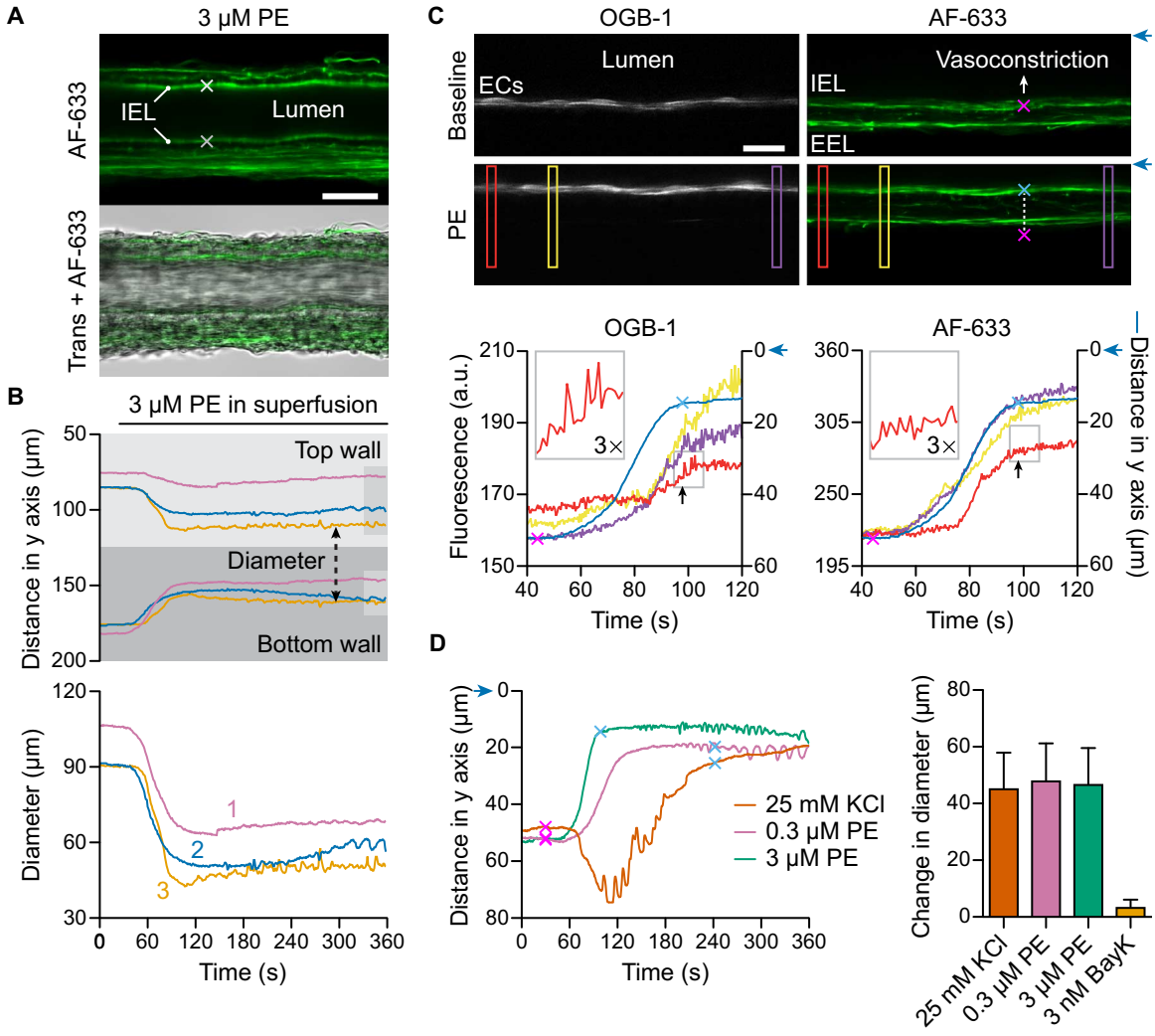

Fig. 7. Defining the trigger point for activation of endothelial cell (EC) Ca^{2+} events during vasoconstriction. (**A**) Confocal images of the top and bottom walls of an arteriole stained with the elastin dye AF-633, indicating the points on the internal elastic lamina (IEL, gray crosses) tracked in the *y* axis over time and the superimposed transmitted light image (Trans); scale bar, 50 μm. (**B**) Original traces showing the tracked IEL in three arterioles (colored lines 1 to 3). The difference between the two traces reflect internal diameter (black dashed line) and are plotted for each arteriole. Phenylephrine (PE) was added to the superfusion solution for the period indicated by the bar. (**C**) Simultaneously acquired confocal images of ECs loaded with the Ca^{2+} indicator OGB-1 and elastin stained with AF-633. Representative fluorescence intensity data are shown as EC Ca^{2+} events and elastin fluorescence corresponding to colored boxes spanning the full range of movement; a.u., arbitrary units. Increased EC Ca^{2+} was observed at the point indicated by the black arrow (inset, 3× zoom of gray box). The tracked movement of the IEL is overlaid for comparison (blue trace in each panel) and corresponds to crosses shown in the images before (magenta) and during (lighter blue) vasoconstriction to 3 μM phenylephrine. EEL, external elastic lamina; scale bar, 30 μm; blue arrows represent 0 μm in the *y* axis. (**D**) Representative time courses of wall movement in response to KCl and phenylephrine in the same arteriole. The starting positions (magenta crosses) reflect myogenic tone, and the threshold to trigger vasoconstrictor-mediated activation of EC Ca^{2+} events is indicated by light blue crosses. Bar graphs summarize the distance moved (extrapolated to an approximated change in diameter) to reach the trigger point for EC Ca^{2+} activation for each vasoconstrictor. Data are means ± SEM of $n = 6$ arterioles from different animals. Myogenic tone, 53.4 ± 2.3%.

amplify both Ca^{2+} and IP_3 signals, a possibility that aligns well with modeling simulations (*30*). However, the crucial point is to unravel what happens in native arterial tissue.

By combining en face (unpressurized) endothelial cell Ca^{2+} measurements with diameter data from pressurized arteries, IP_3 alone has been interpreted as providing the signal to initiate myoendothelial feedback (*17*). However, various concerns limit the conclusions that can be drawn in this study, including the incorrect assumption that en face Ca^{2+} measurements reflect the situation in pressurized (more depolarized) arterioles, and the use of nonspecific IP_3R antagonists xestospongin C and 2-APB (*23*, *24*, *31*). Here, we used heparin in pressurized arterioles to block all IP_3R isoforms in endothelial cells and directly activated smooth muscle L-type VDCCs with BayK. As a result, we visualized distinct, localized endothelial cell Ca^{2+} events, almost always within holes through the internal elastic lamina. These are the sites of myoendothelial contact and represent a unique microdomain that can convey the intercellular passage of Ca^{2+}. Because both Ca^{2+} and IP_3 have binding sites on IP_3Rs, and both are necessary to enable Ca^{2+} release (*32*–*34*), it is reasonable to suggest that, collectively, both may act together as a myoendothelial signal.

A key role for endothelial cell K^+ channels in vasomotion has been demonstrated previously, but without ascribing this role to any particular

channel type (*35*). Physiologically, vasomotion facilitates blood flow control and capillary function in the microcirculation and is disrupted in diseases such as diabetes and hypertension (*36*). The function of IK_{Ca} channels is compromised in these diseases (*37*), which may underpin a lack of vasomotion, a notion that requires further investigation. However, VDCC-driven endothelium-dependent feedback must be considered when assessing the contribution of endothelial cells to systemic blood pressure and when formulating computational models of arteriolar reactivity.

Feedback dilation was only observed after the peak constriction to both phenylephrine and KCl, and this delay is consistent with a threshold point for endothelial cell activation. We ruled out endothelial cell shape change as a major contributing factor to their activation, because the change in diameter to 3 nM BayK was negligible (peak response, <10 μm) and could be further limited with blebbistatin, yet robust, many-fold increases in endothelial cell Ca^{2+} events were stimulated. The extent of depolarization necessary to raise VDCC open probability and trigger the myoendothelial signaling circuit is not clear, but the resting E_m in skeletal muscle arterioles at 80 mmHg is −40 mV (*17*, *38*), and 0.1 μM phenylephrine depolarizes hamster skeletal muscle arterioles by ~10 mV, which is associated with a ~30-μm decrease in diameter (*17*), suggesting that the threshold is less negative than −40 mV. Because the smooth muscle membrane potential dominates that of the endothelium, depolarization would be expected to reduce Ca^{2+} influx across the membranes of endothelial cells because VDCCs are absent in these cells. Thus, the local cytoplasmic concentration achieved adjacent to smooth muscle L-type VDCCs will provide the driving force for Ca^{2+} movement through gap junctions to the endothelium.

Finally, it is important to note that our observations were not complicated by any direct agonist action on endothelial cells, because neither phenylephrine [consistent with (*18*)] nor BayK stimulated a Ca^{2+} response in isolated endothelial cell tubes, correlating with an absence of $Ca_V1.2$. The depolarized resting potential of freshly isolated endothelial cell tubes, ~−20 mV (*39*), should not prevent either the action of phenylephrine (through IP_3Rs) or the ability of BayK to increase VDCC open probability (*6*, *40*, *41*). Thus, it seems reasonable to conclude that in smooth muscle, L-type VDCC activity can alone trigger the intercellular Ca^{2+} circuit.

Physiologically, the endothelium-dependent feedback circuit that we have defined may limit ischemia during periods of sustained sympathetic nerve activity, for example, during exercise, particularly in noncontracting muscle (*42*). Endothelial cell IK_{Ca} channel activity appears to be key, and when their activity is compromised by disease states such as hypertension and diabetes (*37*), negative feedback will be reduced. As a consequence, vascular reactivity will increase compromising blood flow within the skeletal muscle microcirculation, potentially contributing to increases in blood pressure (*43*).

MATERIALS AND METHODS

Animal procedures

Male Wistar rats (Charles River; weight, 240 to 280 g) were anesthetized with urethane (2.8 g/kg intraperitoneally), and the cremaster muscle was exteriorized (*37*), excised, and placed in cold (4°C) Mops-buffered solution containing 145.0 mM NaCl, 4.7 mM KCl, 2.0 mM $CaCl_2$, 1.17 mM $MgSO_4$, 2.0 mM Mops, 1.2 mM NaH_2PO_4, 5.0 mM glucose, 2.0 mM pyruvate, 0.02 mM EDTA, and 2.75 mM NaOH (pH 7.40 ± 0.02 at 37°C). After tissue removal, rats were euthanized using a Schedule 1 procedure [Animals (Scientific Procedures) Act 1986, UK]. Segments of the main intramuscular arteriole (1A) were dissected from the muscle as previously described (*1*, *44*).

Cannulated arteriolar preparation

Isolated rat cremaster arteriolar segments were cannulated at each end with glass micropipettes (external diameter, ~95 μm) and positioned in a 1.5-ml temperature-regulated chamber (RC-27N, Warner Instruments) on the stage of an inverted microscope (IX70 or IX81, Olympus) and continually superfused (2 ml min^{-1}) with Mops-buffered solution. To avoid luminal flow, equal pressure was maintained across the vessel throughout an experiment. Artery segments were warmed to 34°C, gradually pressurized to 80 mmHg, longitudinally straightened to eliminate lateral bowing of the vessel (*1*, *45*), and allowed to develop spontaneous myogenic tone over a 20-min equilibration period. After development of ~50% tone, endothelial cell viability of arterioles was tested by exposure to 0.1, 0.3, and 1 μM acetylcholine; only arterioles dilating >95% of the passive diameter (maximal dilation) were used for experiments. Inner diameter was measured at 1 to 2 Hz either automatically using DiamTrak 3+ version 3.5 (T. O. Neild) (*1*) or manually using a video caliper (Microcirculation Research Institute, Texas A&M University, United States) coupled to a PowerLab 2/20 (AD Instruments) running LabChart version 7.2.2. When one arterial wall was imaged at the midplane, at higher magnification, the movement of the internal elastic lamina during dilation and constriction was tracked using MetaMorph software (version 7.7.4.0, Molecular Devices).

Immunohistochemistry was performed in pressurized arterioles as previously described (*46*). In brief, arterioles were fixed in 2% paraformaldehyde for 10 min at 37°C, washed with phosphate-buffered saline (PBS), and then incubated in blocking buffer [luminal and abluminal, 1% bovine serum albumin (BSA) and 0.1% Tween 20] for 60 min at 37°C and then overnight with primary antibody (pumped into the lumen of the arteriole and added to the bath) at 4°C. The primary antibody is 1:200 mouse monoclonal to $Ca_V1.2$ calcium channel (MAB13170, clone L57/46, Millipore). The following day, the bath solution was replaced with PBS, and the lumen was perfused with an Alexa Fluor 488 secondary antibody [1:100 chicken anti-mouse immunoglobulin G (IgG), A-21200, Invitrogen] and incubated for 2 hours at room temperature. This labeled $Ca_V1.2$ in vascular smooth muscle by diffusion through the arteriolar wall and avoided labeling cells in the adventitia. Nuclei and elastin (including the internal elastic lamina) were stained with 15 μM propidium iodide and 200 nM AF-633 (A-30634, Molecular Probes), respectively (*47*). Arterioles were excited at 488, 546, and 633 nm, and the fluorescence emitted at 505 to 525, 560 to 620, and 655 to 755 nm was acquired through a water immersion objective [40×; numerical aperture (NA), 0.9; working distance (WD), 0.15 mm; Olympus, 1024 × 1024 pixels] using a laser scanning confocal microscope (FV1000, Olympus). z-Stacks through the artery wall were obtained at 0.2-μm increments using FluoView software (FV10-ASW 3.0, Olympus) and reconstructed in Imaris software (version 7.2.3, Bitplane).

Endothelial cell tube isolation procedure

Endothelial cell tubes were isolated as previously described (*1*, *47*) with modifications made to isolate from rat cremaster arterioles. In brief, cremaster tissues were pinned in a dissection dish containing cold (4°C) dissection buffer (pH 7.40 ± 0.02 at 37°C, 285 to 305 mosM) containing 137.0 mM NaCl, 5.6 mM KCl, 1.0 mM $MgCl_2$, 10.0 mM Hepes, 10.0 mM glucose, 0.01 mM sodium nitroprusside, and 0.1% BSA. The main arteriolar branch (1A) in each cremaster was dissected free of surrounding

tissue, one end cannulated by a glass micropipette (~100 μm outer diameter) and the lumen flushed with cold dissection buffer to remove residual blood components. The arterioles were then cut into two to three smaller segments (~1 to 1.5 mm in length) and transferred into a 1.5-ml Axygen MaxyClear snaplock microtube (MCT-150-C, Corning) on ice containing 1 ml of dissection buffer.

To obtain endothelial cell tubes, the collected arteriole segments were then allowed to warm to room temperature (~10 min), and the solution was aspirated and gently replaced with enzyme-free dissociation buffer (pH 7.40 ± 0.02 at 37°C, 285 to 305 mosM) containing 137.0 mM NaCl, 5.6 mM KCl, 1.0 mM $MgCl_2$, 10.0 mM Hepes, 10.0 mM glucose, 2.0 mM $CaCl_2$, and 0.1% BSA to remove residual dissection buffer. This solution was aspirated and replaced with preheated (to 37°C) dissociation buffer containing the following enzymes: papain (0.62 mg ml^{-1}) (P4762, Sigma), dithioerythritol (1.0 mg ml^{-1}) (D8255, Sigma), and collagenase (1.5 mg ml^{-1}) (C8051, Sigma). Arteriole segments were incubated for 25 min at 37°C. The buffer was then aspirated and replaced with room temperature enzyme-free dissociation buffer to terminate the digestion. Arteriole segments were transferred to a 35-mm × 10-mm culture dish (430165, Corning) containing enzyme-free dissociation buffer for trituration. Endothelial cell tubes were dissociated from surrounding smooth muscle cells by gentle trituration using a glass micropipette (4878, World Precision Instruments) with an inner diameter of ~90 to 110 μm. An injector (Nanoliter 2010, ~300 to 500 nl min^{-1}) coupled with a Micro4 controller (World Precision Instruments) was mounted on an upright Olympus BX51WI microscope to allow for real-time visualization of the trituration procedure (*48*).

Freshly isolated endothelial cell tubes were transferred to a 1.5-ml temperature-regulated chamber containing perfusion buffer (pH 7.40 ± 0.02 at 37°C, 285 to 305 mosM) containing 137.0 mM NaCl, 5.0 mM KCl, 1.0 mM $MgCl_2$, 10.0 mM Hepes, 10.0 mM glucose, and 2.0 mM $CaCl_2$. Endothelial cell tubes were pinned on the bottom of the chamber using two round-tipped pinning pipettes (~140- to 160-μm tip diameter) positioned using micromanipulators. Tubes were then stretched to their approximate physiological lengths by adjusting the horizontal tension on the tissue using the micromanipulators. Experiments on endothelial cell tubes were performed at room temperature, because the integrity of the preparation is reduced at higher temperatures (*48*).

Measurement of $[Ca^{2+}]_i$ in pressurized arterioles and endothelial cell tubes

Loading and imaging protocols were performed as previously described (*49*). Pressurized vessels were perfused intraluminally (20 to 30 min) for selective loading of the endothelium or bathed (120 min) at 34°C to load the smooth muscle cells, in both cases with Mops-buffered solution containing filtered (0.2-μm pore) Oregon Green 488 BAPTA-1 AM (OGB-1, 10 or 20 μM, respectively) and 0.0025% pluronic F-127. For simultaneous imaging of both cell types by multiphoton microscopy, endothelial cells were loaded for the last 30 min of the smooth muscle incubation period. In some experiments, arterioles were incubated with 0.1 μM AF-633 (A-30634, Molecular Probes) for 10 min to label elastin. The objective was heated (custom-built Peltier heater, Department of Pharmacology, University of Oxford, UK) to prevent heat loss from the chamber. Endothelial cell tubes were loaded at room temperature with perfusion buffer containing Fluo-4 AM (20 μM) and 0.005% pluronic F-127 for 30 to 35 min. In all instances, excess indicator was washed from the preparation, and the loaded AM form of the dye was allowed to de-esterify and equilibrate. Pressurized arterioles were de-esterified for 30 min, whereas tubes were de-esterified for 10 to 30 min. Only cells responsive to 1 μM acetylcholine were used for analysis.

In most experiments, the fluorescence intensity from loaded endothelial or smooth muscle cells was visualized by lowering the focal plane to cells at the bottom of the pressurized arteriole or endothelial cell tube. Images were obtained using a 40× water immersion objective (40×/1.15-NA objective; WD, 0.25 mm, Olympus; excitation, 488 nm; emission, >505 nm) and were acquired using an Olympus FV500 or FV1000MPE (FluoView version 5.0 or FV10-ASW software, respectively) at ~3 Hz. In two sets of experiments, the focal plane was raised to the midplane of the arteriolar wall. Endothelial cell Ca^{2+} responses and elastin were simultaneously visualized with a Mai Tai DeepSee Ti:Sapphire multiphoton laser (excitation, 790 nm; 2.5%; 1.96 W; pulse width, <80 fs; emission split to capture 495 to 540 nm: OGB-1; emission split to capture 575 to 630 nm: AF-633). To ensure that the field of view included the range of wall movement during exposure to vasoconstrictors, the image size was 512 × 192 pixels, equating to 234 × 88 μm; images were acquired at 2.2 Hz. In these experiments, because only one arterial wall was imaged, the distance moved by the internal elastic lamina during vasoconstriction was doubled to approximate changes in diameter. Using this approach, we could not obtain a value for the frequency of endothelial cell Ca^{2+} events due to arterial motion during vasoconstriction and the lower frequency of acquisition. Instead, multiple ROIs large enough to include the endothelial cells throughout the range of wall positions were used, and the time and therefore *y*-axis position at which oscillations in endothelial cell $[Ca^{2+}]_i$ occurred were monitored both visually and by analysis of average-intensity plots. To establish whether arterial motion per se altered fluorescence intensity, the same ROIs were placed over the elastin channel. Constriction increased fluorescence intensity, which may be due to the concentration of fluorescence in the *z* axis or a relatively thinner distance for laser and/or emitted photon penetration in a smaller-diameter arteriole. Therefore, in these experiments, measurements of OGB-1 fluorescence were limited to observing the onset of endothelial cell Ca^{2+} events (waves). In the second set of experiments, endothelial and smooth muscle cell Ca^{2+} activity were imaged simultaneously by using the multiphoton laser (excitation, 790 nm) and raising the focal plane to the midplane of one side of the arteriolar wall as previously described (*1*); images were acquired at ~3 Hz.

Data were analyzed using MetaMorph software (version 7.7.4.0, Molecular Devices) as previously described using subcellular ROIs (diameter, ~5 μm) (*1*) (fig. S2, A to D). This approach was directly compared to an automated analysis software plugin for ImageJ, used for detection of endothelial cell Ca^{2+} events in intact, unpressurized arteries (LC_Pro) (*50*, *51*). The same TIFF (tagged image file format) stack was used for both automated and manual analyses to compare outputs to visual inspection, and for pressurized arterioles, manual analysis was more accurate (fig. S2, A to D). A major advantage of MetaMorph is the ability to place and move an ROI within a cell in a TIFF image stack and see traces of intensity over time (Region Measurements) on the screen, allowing the user to move the ROI around the entire surface of each individual cell and watch for events. When a deflection was detected, the frames were advanced through that event to confirm that it was not due to an artifact. The point of origin of the event was then marked with an ROI. Once complete, the events were then classified as local if they radiated from a single point and terminated within ~10 μm (value not fixed due to heterogeneous points of origin in varied-shaped endothelial cells) or propagating waves, in which case a second ROI was placed along the cell to establish the

temporal alignment of events. The blue and yellow traces in fig. S2C were defined as waves, and they tended to travel at least half the cell length. The heterogeneity in both endothelial cell shape and the point of origin in each Ca^{2+} event meant that this classification was based on manual analysis of each event, rather than a set distance or surface area. Each event within a given endothelial cell was counted and reported as an overall frequency of Ca^{2+} events, the combined local and wave events. The percentage of active cells was also reported, as well as endothelial cell Ca^{2+} event frequency for the entire frame, the average from active cells only. For midplane experiments, ROIs were placed on three to five active smooth muscle and/or one to two endothelial cells per image stack, and the frequency of Ca^{2+} responses (events per minute) was recorded. For endothelial cell imaging experiments (pressurized arterioles and isolated tubes), all the cells in the field of view (~8 to 15 cells and ~40 to 100 cells, respectively) were individually and manually analyzed for Ca^{2+} event frequency over a ≥60-s acquisition sequence. To analyze experiments in the presence of 30 nM BayK, which induced robust vasomotion (Fig. 6A and movie S1), a TIFF stack of a subset of images was constructed in which the endothelium remained in focus in one field of view. Results are presented as either the frequency (events per minute) reported only from active cells, with the percentage of active cells provided, or F/F_0, calculated by dividing the fluorescence intensity (F) by an average baseline fluorescence intensity (F_0). The number of Ca^{2+} events identified as local or waves was divided by the total number of Ca^{2+} events observed to give percentage local and percentage waves. For endothelial cell Ca^{2+} responses to acetylcholine, the ROI encircled the whole cell, and results from five cells per arteriole were shown as F/F_0 of 2-s averages for each n value.

RNA extraction and RT-qPCR in isolated arterioles and endothelial cell tubes

Arterioles and endothelial cell tubes were isolated as described above, removing residual blood cells by perfusion. For intact arterioles, the central, 1A arterioles from the left and right cremaster tissue of one animal were pooled for each n value and were homogenized using a pellet pestle (47747-370, VWR) in 1.5-ml microtubes (Axygen, MCT-150-C, Corning). RNA was extracted using the RNeasy Plus Mini Kit (74134, Qiagen). For endothelial cell tubes, three >1-mm-long tubes were pooled from one animal for each n value. Upon dissociation from the smooth muscle cells, tubes were transferred using a new glass micropipette into a clean 35-mm × 10-mm culture dish containing dissociation buffer and repeated three more times to reduce smooth muscle cell contamination. RNA was then extracted from the tubes using Cells-to-CT 1-Step TaqMan Kit lysis buffer (A25603, ThermoFisher Scientific).

RT-qPCRs were carried out using the Cells-to-CT kit (A25603, ThermoFisher Scientific). PCRs for each gene were carried out in the same reaction (n = 4 animals for each gene). Gene-specific carboxyfluorescein (FAM)–conjugated TaqMan probes were purchased from ThermoFisher Scientific (table S2). Reverse transcription was performed at 50°C for 20 min, followed by heat activation of Taq polymerase at 95°C for 30 s. PCR was carried out by repeating 95°C for 30 s and then 60°C for 1 min for 40 cycles using the 7500 Fast Real-Time PCR system (4351107, ThermoFisher Scientific). All samples were run in duplicate, and a no-template negative control was included for each gene. Relative gene expression was calculated with the Δ cycle threshold (ΔC_t) method and normalized to both hypoxanthine phosphoribosyltransferase 1 (*Hprt1*) and β-actin (*Actb*) as housekeeping genes. The absence of smooth muscle cells in each tube extraction was assessed by expression of the smooth muscle cell marker α–smooth muscle actin (*Acta2*); in all cases, a C_t value of >36 was considered "not detected."

Addition of vasoconstrictors

A combination of methods was used. Phenylephrine was either directly added to a static bath for rapid responses or added to the superfusion solution until the response equilibrated (~5 min). Isotonic KCl was always added to the superfusion solution and allowed to equilibrate. BayK was added cumulatively (3 and then 27 nM) to a static bath, and because it was not fully reversible, each arteriole was only exposed once to BayK. Consequently, for each set of inhibitor treatments, all functional and endothelial cell Ca^{2+} responses to BayK were obtained in separate arterioles to control experiments. 4-Aminopyridine was always added to a static bath.

Effect of inhibitors and vasoactive agents on endothelial cell Ca^{2+} events

The contribution of VDCC to endothelial cell Ca^{2+} activity was assessed directly, using either the selective antagonist nifedipine (1 μM, 15-min incubation at 5 mmHg after which pressure was raised to 80 mmHg in the continued presence of nifedipine; total of >30-min incubation) or the selective agonist BayK (3 and 30 nM). The effect of arteriolar depolarization on endothelial cell Ca^{2+} activity was assessed using isotonic 25 mM KCl or the nonselective voltage-dependent K^+ channel blocker, 4-aminopyridine (2 mM).

Correlation between BayK-induced Ca^{2+} activity and holes in the internal elastic lamina

Endothelial cell Ca^{2+} events and the internal elastic lamina (myoendothelial microdomain) were imaged simultaneously at ~3 Hz using the 488- and 633-nm visible laser lines on an Olympus FV1000 inverted microscope. Experiments were performed using 3 nM BayK, because this concentration caused a significant increase in endothelial cell Ca^{2+} activity, with limited tissue movement. Regions of endothelial cell Ca^{2+} activity were identified, and the regions were then superimposed on images of the elastin. The number of regions overlapping with holes in internal elastic lamina was divided by the total number of regions to determine the percentage of total events occurring in holes in the internal elastic lamina, as previously described (*1*).

Loading heparin into endothelial cells to inhibit IP_3Rs

Whereas we have previously used pinocytosis to load antibodies into endothelial cells (*52*), the negative charge of heparin made use of TransFectin Lipid Reagent (Bio-Rad, 1703350) possible. When developing the protocol 5(6)-FAM (0.1 mg/ml, 0.27 mM), which is also negatively charged, was used to demonstrate cell loading. Because low–molecular mass (5 kDa) heparin blocks IP_3Rs in both cell homogenates and intact cells (*24*, *53*), we used the same form of heparin (from porcine intestinal mucosa; Fisher, BPE2524; 10 mg/ml, 2 mM). To monitor cell loading and localization with endothelial cells, a Cy5-tagged form of ~12- to 15-kDa heparin (Nanocs Inc., HRN1-S5-1) was used. Hepes-buffered solution (containing 130 mM NaCl, 5.0 mM KCl, 1.2 mM $MgSO_4$, 1.0 mM $CaCl_2$, 10.0 mM Hepes, and 10.0 mM glucose) was used to dissolve the molecule of interest (FAM or heparin), and TransFectin (1 μl/ml) was added (final pH, 7.40 ± 0.02). Solutions were mixed at 20 rpm for 20 min using a rotating wheel (Stuart, SB2) at room temperature before immediate use. A Beehive syringe pump was used to deliver TransFectin solutions into the lumen of arterioles while at low pressure (5 mmHg) at 10 μl/min for 6 min, followed by 0.5 μl/min for

the remainder of the experiment. Images were obtained using a 40× water immersion objective (40×/1.15 NA objective; WD, 0.25 mm, Olympus; excitation, 488 nm and emission, >505 nm for FAM; excitation, 635 nm and emission, 655 to 755 nm for Cy5) and were acquired using Olympus FluoView 1000 software (FV10-ASW). This concentration of TransFectin did not affect myogenic tone or vasodilation to acetylcholine (fig. S4). On the basis of fluorescence intensity, the concentration of FAM loaded into cells was about 1000-fold less than that in the lumen of arterioles. The fluorescence of heparin-Cy5 was not the same in solution as when bound inside cells; therefore, a similar comparison could not be made for heparin concentrations. However, if the loading of heparin were comparable in efficiency to FAM, there would be an amount of heparin (about 10 μg/ml, 2 μM) inside cells that is within the range for effective antagonism of IP_3Rs (*24*, *53*, *54*). In experiments where endothelial cell Ca^{2+} was measured, arterioles were loaded with OGB-1 before TransFectin-heparin. At 5 mg/ml, 5-kDa heparin blocked endothelial cell Ca^{2+} responses to acetylcholine in two of three arterioles, whereas at 10 mg/ml, 5-kDa heparin blocked responses in six of seven arterioles (fig. S4). Once acetylcholine responses were inhibited, arterioles were incubated with AF-633 and pressurized, and endothelial cell Ca^{2+} responses to 3 and 30 nM BayK were determined and aligned with simultaneous images of the internal elastic lamina. In separate experiments, the cellular localization of heparin-Cy5 was compared to the expression of IP_3R1. Arterioles loaded with heparin-Cy5 and elastin stained with Cascade Blue hydrazide (CB-405, 1 μM; excitation, 405 nm; emission, 430 to 460 nm) were imaged (z-stack) at 3× digital zoom immediately before fixation and immunolabeling (see above; primary antibody: 1:200 rabbit polyclonal to human IP_3R1, PA1-901, ThermoFisher Scientific; Alexa Fluor 488 secondary antibody: 1:200 goat anti-rabbit IgG, A-11008, ThermoFisher Scientific). The Cy5 fluorescence was not apparent after fixation; however, the CB-405 staining was visible the following day and was used to identify and align the Cy5 and Alexa Fluor fluorescence signals. Nuclei were stained with propidium iodide (15 μM).

Luminal pumping of 2-APB and xestospongin C

2-APB (100 μM) and xestospongin C (10 μM) were pumped through the lumen of arterioles to inhibit endothelial cell IP_3Rs in preference to smooth muscle IP_3Rs (*1*). 2-APB was continuously delivered during experiments using a Beehive syringe pump at 2 μl min^{-1}, at which flow rate with buffer alone does not affect arteriolar diameter (*17*).

Damage to the endothelium

Endothelial cells were selectively damaged as previously described (*24*). While pressure was lowered to ~5 mmHg, small air bubbles (~2 μl) were pulsed through the lumen of cannulated arterioles until small fragments of cellular debris were observed.

Drugs and solutions

Oregon Green 488 BAPTA-1 AM (OGB-1; O-6807), Fluo-4 AM (Fluo-4; F-14201), pluronic F-127 (P3000MP), AF-633 (A-30634), and Cascade Blue hydrazide (CB-405; C3221) were obtained from Molecular Probes. Xestospongin C (BML-CA409) was from Enzo Life Sciences; apamin (L8407) was obtained from Latoxan. All other drugs were provided by Sigma. TRAM-34 was dissolved in dimethyl sulfoxide (DMSO) (to 1 mM) and then diluted in Mops-buffered solution for experimentation, with special care taken to avoid precipitation while keeping the final DMSO concentration below 1:1000 (which avoids vehicle-associated artifacts). BayK (10 mM), 2-APB (0.1 M), and nifedipine (1 mM) were dissolved in 100% ethanol. Although also used previously (*1*), close inspection revealed that it was not possible to fully dissolve xestospongin C in fresh, anhydrous DMSO to the stock (10 mM) required to prevent vehicle artifacts; 100% ethanol improved solubility and was used. All other stock solutions were prepared in purified water. Inhibitors were added to the incubation solution, and arterioles were equilibrated for >15 min before measurements, if not mentioned specifically.

Data analysis

In all cases, results are summarized as means ± SEM of *n* arterioles, one per animal. Percentage of myogenic tone (at 80 mmHg) was calculated as the percentage of decrease in maximum diameter (D_{Max}) once a stable baseline diameter ($D_{Baseline}$) had been achieved [$(D_{Max} - D_{Baseline})/D_{Max} \times 100$]. When baseline was not stable, the average diameter over a 10-s period was used. The Ca^{2+} event data represent analysis of at least 10 individual cells per arteriole or endothelial cell tube; the values were then averaged to provide one *n* value. Statistical comparisons were made in Prism 7 software (GraphPad) using paired Student's *t* test, one-way analysis of variance (ANOVA), or two-way ANOVA with Bonferroni's post-test as appropriate, where $P < 0.05$ was considered significant. Power analysis was performed using G*Power 3.1 software (*55*) to verify that the sample size gave a value of >0.8 if *P* was >0.05.

SUPPLEMENTARY MATERIALS

www.sciencesignaling.org/cgi/content/full/10/486/eaal3806/DC1

Fig. S1. Myogenic tone relies on L-type VDCCs in arterioles.
Fig. S2. Methods for analyzing endothelial cell Ca^{2+} events in cannulated arterioles.
Fig. S3. Block of arteriole constriction using blebbistatin.
Fig. S4. Characteristics of arteriolar endothelial cell Ca^{2+} events.
Fig. S5. Profile of Ca^{2+} release pathways in arteriolar endothelial cells.
Fig. S6. Loading heparin into arteriolar endothelial cells inhibits IP_3Rs.
Fig. S7. Dichotomous effects of 2-APB.
Fig. S8. Observations on the use of cell-permeant inhibitors of phospholipase C and IP_3Rs.
Fig. S9. Effect of ryanodine on arteriolar Ca^{2+} events.
Fig. S10. Effect of nifedipine on vasoconstriction to phenylephrine.
Fig. S11. Simultaneous imaging of endothelial and smooth muscle cell Ca^{2+} events at the arteriolar midplane.
Fig. S12. Characteristics of arteriole vasoconstriction to phenylephrine.
Fig. S13. Intercellular Ca^{2+} circuit in skeletal muscle arterioles.
Table S1. Effect of nifedipine on vasoconstriction to BayK and KCl.
Table S2. Details of rat genes detected with TaqMan probes.
Movie S1. Time course of endothelial cell Ca^{2+} events in response to BayK in a pressurized arteriole.
Movie S2. Time course of endothelial cell Ca^{2+} events in response to BayK in an isolated tube.
Movie S3. Time course of endothelial cell Ca^{2+} events in response to phenylephrine in an isolated tube.
Movie S4. Time course of endothelial cell Ca^{2+} events in response to KCl in a pressurized arteriole.
Movie S5. Time course of endothelial cell Ca^{2+} events in response to 4-aminopyridine in a pressurized arteriole.
Movie S6. Time course of endothelial cell Ca^{2+} events in response to phenylephrine in a pressurized arteriole.

REFERENCES AND NOTES

1. P. Bagher, T. Beleznai, Y. Kansui, R. Mitchell, C. J. Garland, K. A. Dora, Low intravascular pressure activates endothelial cell TRPV4 channels, local Ca^{2+} events, and IK_{Ca} channels, reducing arteriolar tone. *Proc. Natl. Acad. Sci. U.S.A.* **109**, 18174–18179 (2012).
2. M. H. Laughlin, M. J. Davis, N. H. Secher, J. J. van Lieshout, A. A. Arce-Esquivel, G. H. Simmons, S. B. Bender, J. Padilla, R. J. Bache, D. Merkus, D. J. Duncker, Peripheral circulation. *Compr. Physiol.* **2**, 321–447 (2012).
3. M. A. Hill, Y. Yang, S. R. Ella, M. J. Davis, A. P. Braun, Large conductance, Ca^{2+}-activated K^+ channels (BK_{Ca}) and arteriolar myogenic signaling. *FEBS Lett.* **584**, 2033–2042 (2010).

4. M. A. Hill, G. A. Meininger, Calcium entry and myogenic phenomena in skeletal muscle arterioles. *Am. J. Physiol. Heart Circ. Physiol.* **267**, H1085–H1092 (1994).
5. W. A. Catterall, Structure and regulation of voltage-gated Ca^{2+} channels. *Annu. Rev. Cell Dev. Biol.* **16**, 521–555 (2000).
6. G. Thomas, M. Chung, C. J. Cohen, A dihydropyridine (Bay k 8644) that enhances calcium currents in guinea pig and calf myocardial cells. A new type of positive inotropic agent. *Circ. Res.* **56**, 87–96 (1985).
7. M. T. Nelson, H. Cheng, M. Rubart, L. F. Santana, A. D. Bonev, H. J. Knot, W. J. Lederer, Relaxation of arterial smooth muscle by calcium sparks. *Science* **270**, 633–637 (1995).
8. O. F. Harraz, R. R. Abd El-Rahman, K. Bigdely-Shamloo, S. M. Wilson, S. E. Brett, M. Romero, A. L. Gonzales, S. Earley, E. J. Vigmond, A. Nygren, B. K. Menon, R. E. Mufti, T. Watson, Y. Starreveld, T. Furstenhaupt, P. R. Muellerleile, D. T. Kurjiaka, B. D. Kyle, A. P. Braun, D. G. Welsh, $Ca_V3.2$ channels and the induction of negative feedback in cerebral arteries. *Circ. Res.* **115**, 650–661 (2014).
9. E. B. Westcott, W. F. Jackson, Heterogeneous function of ryanodine receptors, but not IP_3 receptors, in hamster cremaster muscle feed arteries and arterioles. *Am. J. Physiol. Heart Circ. Physiol.* **300**, H1616–H1630 (2011).
10. E. B. Westcott, E. L. Goodwin, S. S. Segal, W. F. Jackson, Function and expression of ryanodine receptors and inositol 1,4,5-trisphosphate receptors in smooth muscle cells of murine feed arteries and arterioles. *J. Physiol.* **590**, 1849–1869 (2012).
11. Y. Yang, T. V. Murphy, S. R. Ella, T. H. Grayson, R. Haddock, Y. T. Hwang, A. P. Braun, G. Peichun, R. J. Korthuis, M. J. Davis, M. A. Hill, Heterogeneity in function of small artery smooth muscle BK_{Ca}: Involvement of the β1-subunit. *J. Physiol.* **587**, 3025–3044 (2009).
12. K. A. Dora, M. P. Doyle, B. R. Duling, Elevation of intracellular calcium in smooth muscle causes endothelial cell generation of NO in arterioles. *Proc. Natl. Acad. Sci. U.S.A.* **94**, 6529–6534 (1997).
13. L. W. M. Nausch, A. D. Bonev, T. J. Heppner, Y. Tallini, M. I. Kotlikoff, M. T. Nelson, Sympathetic nerve stimulation induces local endothelial Ca^{2+} signals to oppose vasoconstriction of mouse mesenteric arteries. *Am. J. Physiol. Heart Circ. Physiol.* **302**, H594–H602 (2012).
14. J. Ledoux, M. S. Taylor, A. D. Bonev, R. M. Hannah, V. Solodushko, B. Shui, Y. Tallini, M. I. Kotlikoff, M. T. Nelson, Functional architecture of inositol 1,4,5-trisphosphate signaling in restricted spaces of myoendothelial projections. *Proc. Natl. Acad. Sci. U.S.A.* **105**, 9627–9632 (2008).
15. K. A. Dora, J. M. Hinton, S. D. Walker, C. J. Garland, An indirect influence of phenylephrine on the release of endothelium-derived vasodilators in rat small mesenteric artery. *Br. J. Pharmacol.* **129**, 381–387 (2000).
16. Y. Kansui, C. J. Garland, K. A. Dora, Enhanced spontaneous Ca^{2+} events in endothelial cells reflects signalling through myoendothelial gap junctions in pressurized mesenteric arteries. *Cell Calcium* **44**, 135–146 (2008).
17. C. H. Tran, M. S. Taylor, F. Plane, S. Nagaraja, N. M. Tsoukias, V. Solodushko, E. J. Vigmond, T. Furstenhaupt, M. Brigdan, D. G. Welsh, Endothelial Ca^{2+} wavelets and the induction of myoendothelial feedback. *Am. J. Physiol. Cell Physiol.* **302**, C1226–C1242 (2012).
18. W. F. Jackson, E. M. Boerman, E. J. Lange, S. S. Lundback, K. D. Cohen, Smooth muscle α_{1D}-adrenoceptors mediate phenylephrine-induced vasoconstriction and increases in endothelial cell Ca^{2+} in hamster cremaster arterioles. *Br. J. Pharmacol.* **155**, 514–524 (2008).
19. A. C. Straub, A. C. Zeigler, B. E. Isakson, The myoendothelial junction: Connections that deliver the message. *Physiology (Bethesda)* **29**, 242–249 (2014).
20. N. L. Allbritton, T. Meyer, L. Stryer, Range of messenger action of calcium ion and inositol 1,4,5- trisphosphate. *Science* **258**, 1812–1815 (1992).
21. G. D. Dickinson, K. L. Ellefsen, S. P. Dawson, J. E. Pearson, I. Parker, Hindered cytoplasmic diffusion of inositol trisphosphate restricts its cellular range of action. *Sci. Signal.* **9**, ra108 (2016).
22. L. Leybaert, IP_3, still on the move but now in the slow lane. *Sci. Signal.* **9**, fs17 (2016).
23. D. Bai, C. del Corsso, M. Srinivas, D. C. Spray, Block of specific gap junction channel subtypes by 2-aminoethoxydiphenyl borate (2-APB). *J. Pharmacol. Exp. Ther.* **319**, 1452–1458 (2006).
24. H. Saleem, S. C. Tovey, T. F. Molinski, C. W. Taylor, Interactions of antagonists with subtypes of inositol 1,4,5-trisphosphate (IP_3) receptor. *Br. J. Pharmacol.* **171**, 3298–3312 (2014).
25. A. W. Moore, S. E. Bearden, S. S. Segal, Regional activation of rapid onset vasodilatation in mouse skeletal muscle: Regulation through α-adrenoreceptors. *J. Physiol.* **588**, 3321–3331 (2010).
26. Y. Yang, Y. Sohma, Z. Nourian, S. R. Ella, M. Li, A. Stupica, R. J. Korthuis, M. J. Davis, A. P. Braun, M. A. Hill, Mechanisms underlying regional differences in the Ca^{2+} sensitivity of BK_{Ca} current in arteriolar smooth muscle. *J. Physiol.* **591**, 1277–1293 (2013).
27. W. F. Jackson, K. L. Blair, Characterization and function of Ca^{2+}-activated K^+ channels in arteriolar muscle cells. *Am. J. Physiol.* **274**, H27–H34 (1998).
28. B. E. Isakson, S. I. Ramos, B. R. Duling, Ca^{2+} and inositol 1,4,5-trisphosphate–mediated signaling across the myoendothelial junction. *Circ. Res.* **100**, 246–254 (2007).
29. B. E. Isakson, Localized expression of an Ins(1,4,5)P_3 receptor at the myoendothelial junction selectively regulates heterocellular Ca^{2+} communication. *J. Cell Sci.* **121**, 3664–3673 (2008).
30. S. Nagaraja, A. Kapela, N. M. Tsoukias, Intercellular communication in the vascular wall: A modeling perspective. *Microcirculation* **19**, 391–402 (2012).
31. H. Ozaki, M. Hori, Y.-S. Kim, S.-C. Kwon, D.-S. Ahn, H. Nakazawa, M. Kobayashi, H. Karaki, Inhibitory mechanism of xestospongin-C on contraction and ion channels in the intestinal smooth muscle. *Br. J. Pharmacol.* **137**, 1207–1212 (2002).
32. I. Bezprozvanny, J. Watras, B. E. Ehrlich, Bell-shaped calcium-response curves of Ins(1,4,5) P3- and calcium-gated channels from endoplasmic reticulum of cerebellum. *Nature* **351**, 751–754 (1991).
33. T. Michikawa, J. Hirota, S. Kawano, M. Hiraoka, M. Yamada, T. Furuichi, K. Mikoshiba, Calmodulin mediates calcium-dependent inactivation of the cerebellar type 1 inositol 1,4,5-trisphosphate receptor. *Neuron* **23**, 799–808 (1999).
34. E. C. Thrower, E. J. Lea, A. P. Dawson, The effects of free $[Ca^{2+}]$ on the cytosolic face of the inositol (1,4,5)-trisphosphate receptor at the single channel level. *Biochem. J.* **330**, 559–564 (1998).
35. J. R. H. Mauban, W. G. Wier, Essential role of EDHF in the initiation and maintenance of adrenergic vasomotion in rat mesenteric arteries. *Am. J. Physiol. Heart Circ. Physiol.* **287**, H608–H616 (2004).
36. C. Aalkjær, D. Boedtkjer, V. Matchkov, Vasomotion—What is currently thought? *Acta. Physiol.* **202**, 253–269 (2011).
37. M. Félétou, Endothelium-dependent hyperpolarization and endothelial dysfunction. *J. Cardiovasc. Pharmacol.* **67**, 373–387 (2016).
38. N. Kotecha, M. A. Hill, Myogenic contraction in rat skeletal muscle arterioles: Smooth muscle membrane potential and Ca^{2+} signaling. *Am. J. Physiol. Heart Circ. Physiol.* **289**, H1326–H1334 (2005).
39. E. J. Behringer, S. S. Segal, Tuning electrical conduction along endothelial tubes of resistance arteries through Ca^{2+}-activated K^+ channels. *Circ. Res.* **110**, 1311–1321 (2012).
40. M. C. Sanguinetti, D. S. Krafte, R. S. Kass, Voltage-dependent modulation of Ca channel current in heart cells by Bay K8644. *J. Gen. Physiol.* **88**, 369–392 (1986).
41. J. F. Worley, J. M. Quayle, N. B. Standen, M. T. Nelson, Regulation of single calcium channels in cerebral arteries by voltage, serotonin, and dihydropyridines. *Am. J. Physiol* **261**, H1951–H1960 (1991).
42. M. J. Joyner, G. D. Thomas, Having it both ways? Vasoconstriction in contracting muscles. *J. Physiol.* **550**, 333 (2003).
43. H. Si, W.-T. Heyken, S. E. Wölfle, M. Tysiac, R. Schubert, I. Grgic, L. Vilianovich, G. Giebing, T. Maier, V. Gross, M. Bader, C. de Wit, J. Hoyer, R. Köhler, Impaired endothelium-derived hyperpolarizing factor-mediated dilations and increased blood pressure in mice deficient of the intermediate-conductance Ca^{2+}-activated K^+ channel. *Circ. Res.* **99**, 537–544 (2006).
44. P. Bagher, S. S. Segal, The mouse cremaster muscle preparation for intravital imaging of the microcirculation. *J. Vis. Exp.* **2011**, 2874 (2011).
45. I. N. McSherry, S. L. Sandow, W. B. Campbell, J. R. Falck, M. A. Hill, K. A. Dora, A role for heterocellular coupling and EETs in dilation of rat cremaster arteries. *Microcirculation* **13**, 119–130 (2006).
46. T. O. Neild, Measurement of arteriole diameter changes by analysis of television images. *Blood Vessels* **26**, 48–52 (1989).
47. K. A. Dora, N. T. Gallagher, A. McNeish, C. J. Garland, Modulation of endothelial cell $K_{Ca}3.1$ channels during endothelium-derived hyperpolarizing factor signaling in mesenteric resistance arteries. *Circ. Res.* **102**, 1247–1255 (2008).
48. M. J. Socha, S. S. Segal, Isolation of microvascular endothelial tubes from mouse resistance arteries. *J. Vis. Exp.* **2013**, e50759 (2013).
49. M. J. Socha, C. H. Hakim, W. F. Jackson, S. S. Segal, Temperature effects on morphological integrity and Ca^{2+} signaling in freshly isolated murine feed artery endothelial cell tubes. *Am. J. Physiol. Heart Circ. Physiol.* **301**, H773–H783 (2011).
50. M. Francis, J. Waldrup, X. Qian, M. S. Taylor, Automated analysis of dynamic Ca^{2+} signals in image sequences. *J. Vis. Exp.* **2014**, e51560 (2014).
51. M. Francis, J. R. Waldrup, X. Qian, V. Solodushko, J. Meriwether, M. S. Taylor, Functional tuning of intrinsic endothelial Ca^{2+} dynamics in swine coronary arteries. *Circ. Res.* **118**, 1078–1090 (2016).
52. S. Mather, K. A. Dora, S. L. Sandow, P. Winter, C. J. Garland, Rapid endothelial cell–selective loading of connexin 40 antibody blocks endothelium-derived hyperpolarizing factor dilation in rat small mesenteric arteries. *Circ. Res.* **97**, 399–407 (2005).
53. P. F. Worley, J. M. Baraban, S. Supattapone, V. S. Wilson, S. H. Snyder, Characterization of inositol trisphosphate receptor binding in brain. Regulation by pH and calcium. *J. Biol. Chem.* **262**, 12132–12136 (1987).
54. S. Boitano, E. R. Dirksen, M. J. Sanderson, Intercellular propagation of calcium waves mediated by inositol trisphosphate. *Science* **258**, 292–295 (1992).
55. F. Faul, E. Erdfelder, A.-G. Lang, A. Buchner, G*Power 3: A flexible statistical power analysis program for the social, behavioral, and biomedical sciences. *Behav. Res. Methods* **39**, 175–191 (2007).

Acknowledgments: We thank R. Mitchell for help in preparing figures. **Funding:** C.J.G. holds a Royal Society Wolfson Merit Award. This work was supported by the Wellcome Trust (089815/Z/09/Z), British Heart Foundation (BHF) (grant numbers FS/08/033/25111, FS/13/16/30199, and IG/13/5/30431), and the Oxford BHF Centre of Research Excellence (RE/13/1/30181). K.A.D. is a BHF-funded Senior Basic Science Research Fellow. **Author contributions:** C.J.G., P.B., and K.A.D. designed the research; P.B., C.P., X.Y., H.A.L.L., L.B., and K.A.D. performed the experiments and analyzed the data. C.J.G., P.B., and K.A.D. wrote and edited the manuscript. **Competing interests:** The authors declare that they have no competing interests.

Submitted 10 November 2016
Accepted 15 June 2017
Published 4 July 2017
10.1126/scisignal.aal3806

Citation: C. J. Garland, P. Bagher, C. Powell, X. Ye, H. A.L. Lemmey, L. Borysova, K. A. Dora, Voltage-dependent Ca^{2+} entry into smooth muscle during contraction promotes endothelium-mediated feedback vasodilation in arterioles. *Sci. Signal.* **10**, eaal3806 (2017).

Science Signaling

Voltage-dependent Ca^{2+} entry into smooth muscle during contraction promotes endothelium-mediated feedback vasodilation in arterioles

Christopher J. Garland, Pooneh Bagher, Chloe Powell, Xi Ye, Hamish A. L. Lemmey, Lyudmyla Borysova and Kim A. Dora

Sci. Signal. **10** (486), eaal3806.
DOI: 10.1126/scisignal.aal3806

Ca^{2+}, the intercellular signal in arterioles

Vasoconstriction must be balanced with vasodilation, particularly in the arterioles that supply tissues with blood. Endothelial cells protrude through holes in the internal elastic lamina in arterioles to make contact with vascular smooth muscle cells. Gap junctions are present at these sites where endothelial cells meet vascular smooth muscle cells. IP_3 has been thought to be a signal that passes through these gap junctions to endothelial cells to mediate vasodilation. However, Garland *et al*. showed that it was Ca^{2+}, rather than IP_3, that entered vascular smooth muscle cells through voltage-gated Ca^{2+} channels, subsequently passed through gap junctions into endothelial cells, and initiated vasodilation mediated by endothelial cells. The magnitude of these Ca^{2+} signals in endothelial cells depended on IP_3 receptors. These results resolve a long-standing controversy over how vascular smooth muscle cells communicate with endothelial cells to trigger feedback vasodilation.